Triplet Properties and Interactions of the Primary Electron Donor and Antenna Chromophores in Membranes of *Heliobacterium chlorum*, Studied with ADMR Spectroscopy†

J. Vrieze, E. J. van de Meent, and A. J. Hoff*

Department of Biophysics, Huygens Laboratory, Leiden University, P.O. Box 9504, 2300 RA Leiden, The Netherlands

Received May 21, 1998; Revised Manuscript Received July 16, 1998

ABSTRACT: The triplet states of antenna and reaction center bacteriochlorophyll (BChl) *g* in membranes of *Heliobacterium chlorum* were studied by optically detected magnetic resonance in zero magnetic field, using absorbance detection. A variety of triplet states was detected, which were all localized on single BChl *g* chromophores as concluded from a comparison with the triplet state of monomeric BChl *g* in organic solvents. With the aid of the microwave-induced absorbance difference spectra, we assign a triplet state with zero-field splitting parameters $|D| = 727.5$ and $|E| = 254.5$ MHz to that of the primary donor. The low $|E|$ value indicates that the BChls of the primary donor are monoligated. The intensities of the zero-field transitions were strongly dependent on the redox state of the secondary electron acceptors. A triplet state with $|D| = 690-705$ MHz and $|E| = 230$ MHz, present under all redox conditions, is associated with antenna BChl *g* absorbing at 814 nm. Its triplet yield was independent of the redox conditions; we conclude therefore that the antenna chromophores absorbing at 814 nm are not connected with the reaction center at cryogenic temperatures (1.2 K). In addition, relatively strong signals were detected belonging to triplet states with $|D|$ and $|E|$ of 663−680 and 220−227 MHz, respectively, whose amplitudes were dependent on the redox conditions. Triplet states with these zero-field splitting parameters are located on antenna chromophores absorbing between 798−814 nm; their zero-field transitions and absorbance difference spectra indicate a considerable heterogeneity. The concentration of triplet states of antenna chromophores absorbing around 800 nm decreased markedly upon prolonged excitation at 1.2 K. This phenomenon is attributed to quenching of excitations on antenna pigments by stable charge separation in the closely connected reaction center, possibly involving a low-quantum yield menaquinone electron acceptor.

Heliobacteria is a recently discovered family of photosynthetic bacteria characterized by having BChl *g* as their major pigment (*1*). They mostly live in soil, rice paddies seemingly being their favored habitat, and are strictly anaerobic nitrogen fixers. Of the five species now identified (*2*), *Heliobacterium (H.) chlorum*, the first species discovered (*3*), is one of the most extensively investigated (see, for recent reviews, refs *2* and *4*). On the basis of 16S rRNA analysis, the species belongs to the Gram-positive bacteria, and thus is phylogenetically closer to the Bacillacea than to other phototrophic bacteria (*5*). Of all photosynthetic bacteria, it is closest to the cyanobacteria (*2*). The major subunit of the antenna−reaction center (RC)[1] complex is a single polypeptide of 68 kD, which shows about 20% homology with the two polypeptides of the reaction center core complex of photosystem I (*6*−*8*). Apparently, the Heliobacteria and photosystem I have a common ancestor, which presumably is closer to the Heliobacteria than to photosystem I (because in the latter gene duplication offered more freedom for nonlethal mutation).

The two 68 kD polypeptides constituting the homodimeric antenna−RC complex of *H. chlorum* bind ca. 34 BChls *g*, and two BChl *g*′ molecules (the 13^2 epimer of BChl *g*), the latter possibly forming the (homodimeric) primary electron donor (*9*), and two to three 4,4′-diaponeurosporene molecules (*11*). In addition, two 8^1−OH Chl *a* molecules are present (*12*, *13*), which probably function as primary electron acceptors (A_0), analogous to the acceptor Chl *a* in the green sulfur bacteria and in photosystem I (*14*−*17*). Note that because of the strictly symmetric homodimeric architecture of the antenna−RC complex, there is no reason to assume that there is only one active electron-transport chain as in the purple photosynthetic bacteria.

Also beyond the 8^1−OH Chl *a* electron acceptor, the acceptor side of the heliobacterial RC has some similarity to that of photosystem I, with two or possibly three iron−sulfur centers acting as electron acceptors (*6*, *18*−*22*, *24*). Several menaquinone molecules are present in membrane preparations of *H. chlorum*, and the isolated antenna−RC

† This work was supported by The Netherlands Foundation for Chemical Research SON, and financed by The Netherlands Organization for Scientific Research NWO.

* To whom correspondence should be addressed. Fax +31-71-5275819. E-mail: hoff@biophys.leidenuniv.nl.

[1] Abbreviations: ADMR, absorbance-detected magnetic resonance; A_0, primary (chlorophyll) acceptor; (LD-) $T - S$ (linear-dichroic) triplet-minus-singlet; P_{700}, primary donor of photosystem I; P, primary donor of *Heliobacterium chlorum*; Q, low-quantum yield acceptor; RC, reaction center; X, secondary acceptor; zf(s), zero-field (splitting).

10.1021/bi981207w CCC: $15.00 © 1998 American Chemical Society
Published on Web 09/26/1998

complex of *Heliobacillus mobilis* contains a single menaquinone (*6*, *25*). Reduced quinone may be photoaccumulated (*19*, *20*), but function as an obligatory secondary electron acceptor is put in doubt by extraction experiments, which removed essentially all menaquinone, yet left electron transport properties intact (*26*).

The spectral properties of the antenna−RC complex of the Heliobacteria are dominated by the absorbance bands of BChl *g*, which, like BChl *b*, has an ethylidene group at C8 of ring II, but a vinyl group at C3 of ring I, like Chl *a*. In acetone, the $Q_Y-(S_1 \leftarrow S_0)$ and $Q_X-(S_2 \leftarrow S_0)$ transitions of BChl *g* are at 761.6 and 566.4 nm, respectively, with similar values for BChl *g*′ (*9*). In the antenna−RC complex, there are several spectrally different antenna species, with Q_Y-bands around 790 nm. At 77 K, three components are resolved, centered at 778, 793, and 808 nm (*27*). At cryogenic temperatures, excitation energy within the antenna system is efficiently transferred to antenna chromophores absorbing at the longest wavelength, the antenna B808, which have their maximum fluorescence at 818 nm (*27*). Although the primary donor (P) in the RC absorbs at a considerably shorter wavelength, 794 nm, excitation transfer from the antenna to P at physiological temperatures seems to proceed via the B808 antenna with equal efficiency for all antenna chromophores (*28*, *29*).

When electron transport to the secondary acceptors is blocked, the charges on $P^+A_0^-$ recombine to the triplet state of P (^{3}P) with a yield of 25−30% at 6 K (*17*). With EPR (*21*, *22*) and optical spectroscopy (*17*, *21*, *28*) two distinct triplet states have been observed: the triplet state of P and a triplet state formed by intersystem crossing on antenna chromophores absorbing at 814 nm, which form part of the B808 antenna complex. The zero-field splitting (zfs) parameters of the two triplet states obtained by EPR are the subject of discussion (*21*, *22*).

Because in many respects the small antenna−RC core of the Heliobacteria resembles the antenna core of photosystem I, it is often viewed as a paradigm for this much larger and more complex photosystem. Yet, from the above survey, it is apparent that care must be exerted in drawing the analogy too far. There is a clear need for a more precise delineation of the similarities and the differences between the photosystem of the Heliobacteria and photosystem I of plants. In the present communication, we report an investigation with absorbance-detected magnetic resonance (ADMR) of triplet states of the antenna and primary donor BChl *g* (BChl *g*′) pigments of membrane complexes of *H. chlorum*. Triplet states are sensitive probes of pigment structure and environment, through their magnetic resonance properties (zfs parameters, sublevel decay rates) and their optical interactions with neighboring pigments. The ADMR method is especially useful because it combines the selectivity and sensitivity of optical spectroscopy with the high resolution of magnetic resonance in zero magnetic field (reviewed in ref *30*).

We have unequivocally determined the zfs parameters of the primary donor and of several antenna triplet states. The latter triplets are all located on antenna BChl *g* pigments absorbing at longer wavelengths than the primary donor, indicating inefficient energy transfer from those pigments to the donor at the temperature of the measurement (1.2 K). The zfs parameters of the donor and antenna triplets are all close to those of monomeric BChl *g* in vitro, strongly suggesting that they are localized on single BChl *g* (BChl *g*′) molecules. This allows us to conclude that the primary donor is a weakly coupled dimer. From detailed ADMR-monitored triplet minus singlet ($T - S$) absorbance difference spectra, we conclude that the donor is weakly coupled to the 8^1−OH Chl *a* primary acceptor, absorbing at 670 nm. We compare our results with those of a similar study on photosystem I (*31*) and show that the configuration of the primary electron acceptor is quite similar. Thus, our results support the notion that the Heliobacteria constitutes a suitable model system for the antenna−RC complex of photosystem I with the advantages of a much smaller antenna size and an isolation procedure without the use of detergents.

MATERIALS AND METHODS

ADMR spectroscopy is treated in some depth in ref *30*. Briefly, microwaves resonant between two of the three (zero-field) sublevels of a triplet state generated by continuous illumination transfer population between sublevels having different equilibrium populations and rates of decay to the singlet ground state and, therefore, change the equilibrium concentration of the triplet state. This change is monitored via the ground-state absorbance. The experiment is carried out at very low temperature (here 1.2 K) to inhibit spin−lattice relaxation that competes with microwave-induced transitions. The relative change in absorbance ($\Delta A/A$) is small and, to good approximation, equal to the relative change in transmittance ($\Delta I/I$), which is proportional to the difference in equilibrium populations *and* decay rates of the two levels (u, v) connected by the resonant microwaves: $\Delta I/I \alpha (k_u - k_v)(n_u - n_v)/(k_u + k_v)$. The sign of ΔI must, therefore, be ascertained by a separate experiment in which the sign of the change in absorbance following a brief pulse of resonant microwaves is determined. Generally two types of spectra are measured. (a) The ADMR spectrum is measured in which the microwave frequency is varied while monitoring the absorbance at a fixed suitable wavelength. For each different triplet state, a maximum of three resonances is observed, corresponding to the $|D| + |E|$, $|D| - |E|$ and $2|E|$ zf splittings. (b) The $T - S$ spectrum is measured in which the wavelength of absorption is varied, keeping the microwave frequency fixed at one of the ADMR resonances. The $T - S$ spectrum displays the bleaching of absorbance band(s) of the molecule on which the triplet state is generated, positive bands due to triplet−triplet absorptions, and band shifts of chromophores interacting with the triplet-carrying molecule. Together, the ADMR and $T - S$ spectra form a 2D spectral matrix, from which detailed information can be obtained on the identity and properties of triplet states in complex chromophore arrays, and on chromophore−chromophore interactions in such arrays. In turn, this information gives insight in the architecture of the antenna−reaction center complexes in photosynthetic systems (reviewed in refs *30*, *32*, and *33*).

A tungsten−iodine lamp (250 W) was used for broadband excitation and for measuring transmittance. The transmitted light, passing a monochromator (resolution set at 2−4 nm), was detected by a Peltier-cooled silicon photodiode (RCA 30842). The ADMR setup was essentially as described (*30*, *34*, *35*). The change in transmittance induced by amplitude modulation of the microwaves (312

Hz) was phase-sensitive detected with a lock-in amplifier (SR 510). Microwaves, generated by a HP8350B sweep oscillator with HP83525A plug-in at the maximal output power (~100 mW), were fed into a helix surrounding the sample cuvette. For the linear-dichroic ADMR experiments, a tunable split-ring cavity was placed around the sample cuvette (*36*), such that the microwave magnetic field was perpendicular to the light beam.

Response recovery curves were obtained by applying microwave pulses with a width of 20 μs and a repetition rate of 33 Hz (EG&G 9650 pulse generator and HP33190B microwave switch). The microwaves were amplified by an IFI wide-band amplifier (M5580) and were frequency modulated with 100 kHz through the ADMR band. The change in transmittance induced by the microwave pulses was determined by feeding the output of the photodiode into a differential amplifier (Tektronix AM 502) and averaging the signals by a Nicolet 527.

Heliobacterial membranes were prepared as described in ref *7*. The optical absorption spectrum had a ratio of the absorbance at 788 nm to that at 670 nm of 6.7 or better at room temperature, checked before and after each measurement.

Strongly reducing conditions were obtained by diluting the sample in 100 mM CAPS buffer (pH 10.5−11) that contained 30 mM sodium ascorbate and 30 mM sodium dithionite. The sample was frozen under illumination from 240 K down to 77 K. Under this condition, a relatively large part of the iron−sulfur (secondary) acceptors is reduced (*21*, *22*), and at low temperatures, ^{3}P is formed by radical recombination of $P^+A_0^-$ in 55 ns (*17*). The results were compared with those obtained when the same sample was frozen in the dark. Weakly reducing conditions were obtained by diluting the membranes in 30 mM Tris buffer (pH 8) containing 30 mM sodium ascorbate and freezing the samples in the dark. For comparison, the same sample was also frozen under illumination. Thus, samples were prepared for four reducing conditions: weak−dark-frozen, weak−light-frozen, strong−dark-frozen, and strong−light-frozen.

The absorbance at 788 nm was typically 0.2−0.5 in a 1 mm Perspex cuvette at room temperature, after the addition of 65% (v/v) glycerol to obtain a clear glass upon freezing. The experiments were carried out at ~1.2 K in a bath cryostat. The absorbance spectra were recorded at 6 K in a helium flow cryostat using a spectrophotometer as described (*37*).

RESULTS

Zero-Field Splitting Parameters of Triplet States in Membranes of H. chlorum. For membranes of *H. chlorum*, the change in transmittance as a function of the microwave frequency is shown in Figure 1 for several detection wavelengths within the Q_Y-absorption band. Microwave-induced absorbance difference signals occur at ~450, ~466−476, 490, 509, 883, 906, ~935, 960, and 982 MHz; they represent transitions between various zero-field (*x*, *y*, and *z*) triplet sublevels. The presence of more than three zf transitions and the observation that the relative intensities of the transitions depend on the wavelength of detection selected within the Q_Y-band point to the existence of several triplet states in the photosynthetic apparatus of *H. chlorum*.

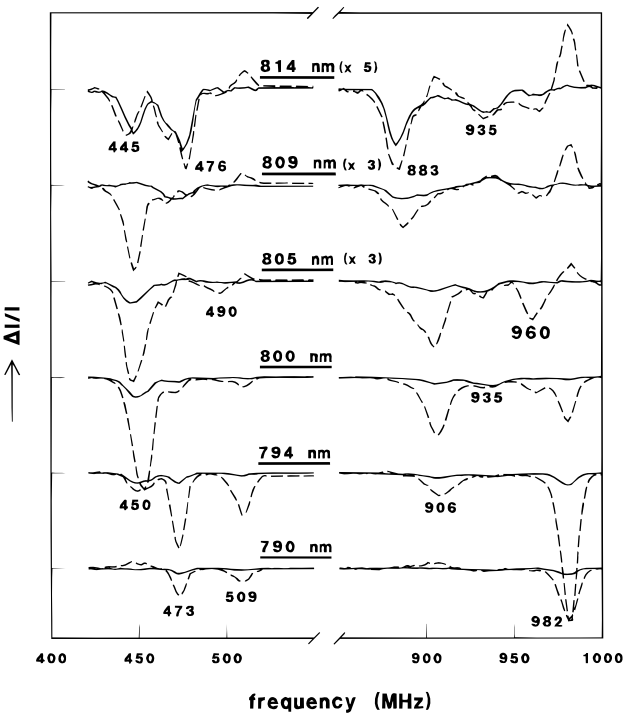

FIGURE 1: ADMR spectra recorded at various wavelengths within the Q_Y band of membranes of *H. chlorum* under weakly (solid line) reducing conditions and frozen in the dark, and under strongly (dashed line) reducing conditions and frozen during illumination. A negative signal corresponds with a decrease in transmittance. Note the difference in vertical scale of the spectra recorded at 805, 809, and 814 nm.

Different reducing conditions result in different relative intensities of the zf transitions. Figure 1 shows the results for the two of the sample conditions mentioned in the Materials and Methods. Membranes suspended in Tris buffer (pH 8, containing 10 mM sodium ascorbate) and frozen in the dark yielded the lowest signal intensities (Figure 1, solid line). When the same samples were thawed and subsequently frozen under illumination, an increase by a factor of 3−4 was observed for the zf transitions at 450, 473, 509, 906, and 982 MHz (not shown). The highest increment of these signals was obtained for dithionite-containing samples (CAPS buffer, pH 10.5, 10 mM sodium ascorbate, and 10 mM sodium dithionite) frozen under illumination. This reducing condition resulted in an increase by a factor of 5−7 at 450, 473, 509, 906, and 982 MHz (Figure 1, dashed line). When the latter samples were frozen in the dark, the amplitude of these signals increased by only 10−20% compared to the membranes frozen in the dark in the absence of dithionite (not shown). We therefore conclude that the addition of dithionite results in only a small amount of reduced secondary acceptors and that photoaccumulation, in the presence of dithionite, is necessary for reducing the secondary acceptors, in agreement with the EPR results of ref *22*. For both samples, freezing the same sample in the dark or under illumination did not affect the intensity of the zf transitions at ~445 and 920−935 MHz at a detection wavelength of 814 nm.

The response of the transmittance following a brief microwave pulse was detected at each zf transition, at a wavelength corresponding to the maximum of the absorbance difference signal for the two reducing conditions of the experiments shown in Figure 1. Some of the measured

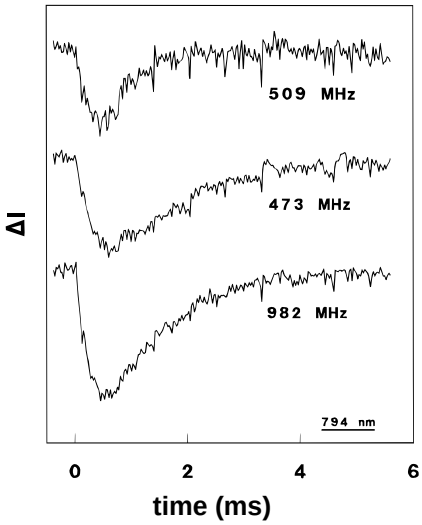

FIGURE 2: Response of the transmittance at 794 nm following a brief microwave pulse at various resonant microwave frequencies, for samples under strongly reducing conditions and frozen during illumination.

recovery curves are displayed in Figure 2. They show a decrease in transmittance followed by a slow recovery to the steady-state level and can be fitted by a sum of two exponentials of opposite sign representing the decay times of the two triplet sublevels connected by the microwaves (*30*). The zfs-parameters, $|D|$ and $|E|$, and the lifetimes of the triplet sublevels are summarized in Table 1, together with results for BChl *g* dissolved in organic solvents (*38*). The assigments of the zf transitions (Table 1) follow from the microwave-induced absorbance difference spectra recorded at the resonant microwave frequencies under different reducing conditions, which will be discussed in the following sections.

The Triplet State of the Primary Donor. Figure 3 shows the microwave-induced absorbance difference spectra recorded at 473, 509, and 982 MHz for samples frozen under strongly reducing conditions in the dark and under illumination (see Materials and Methods). The spectra for weakly reducing conditions, though weaker, were identical in shape (not shown). The signals with negative sign are due to an increase in ground-state absorption (decrease in transmittance). The relatively broad positive signals are attributed to triplet−triplet absorptions, narrower, positive signals to band shifts caused by a change of the interaction between the triplet-carrying chromophore and adjacent chromophores

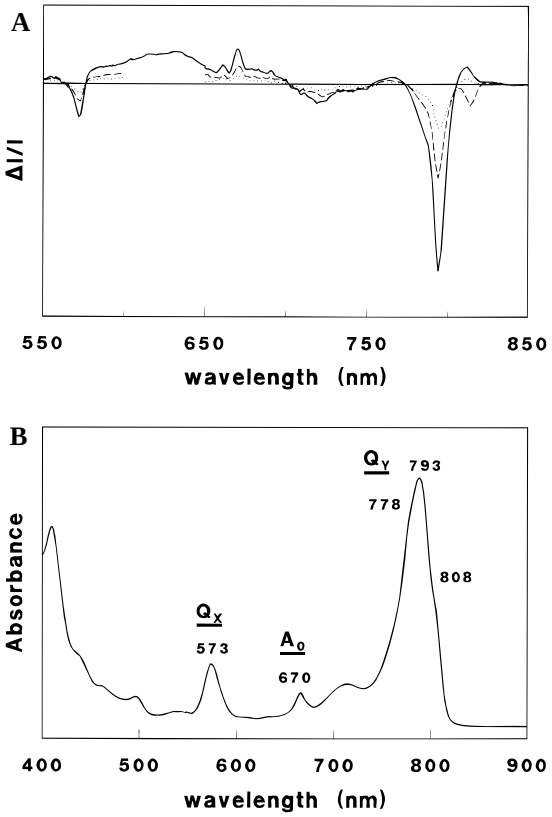

FIGURE 3: (A) Microwave-induced absorbance difference spectra of membranes of *H. chlorum* under strongly reducing conditions and frozen during illumination recorded at 982 MHz (solid line), 509 MHz (dotted line), and 473 MHz (dashed line). (B) Absorbance spectrum recorded at 5 K.

upon triplet formation. Apart from a component at 805−815 nm (see below), the $T - S$ spectra have the same shape, from which we conclude that the zf transitions at 473, 509, and 982 MHz belong to the same triplet state, located on chromophores absorbing at 794 nm. This observation and the increase of the ADMR signal when the sample is frozen under illumination strongly suggest that the spectra represent $T - S$ spectra of ^{3}P formed by radical recombination. This assignment is supported by the fact that the shape of the ADMR-detected $T - S$ spectra at 509 or 982 MHz is similar to that of the flash-induced $T - S$ spectrum of ^{3}P reported in refs *17* and *28*. The positive signal at 805−815 nm and the signal at 670 nm (see below) in the ADMR-detected $T - S$ spectrum were not observed in the flash-induced $T - S$ spectrum, probably because the selectivity with resonant microwaves used in ADMR allows a better discrimination

Table 1: Zero Field-Splitting Parameters D and E (in megahertz, Error ± 0.5 MHz) and Sublevel Decay Times τ_i (in milliseconds) of the Triplet States in Membranes of *H. chlorum* and of ^{3}BChl *g* in Organic Solvents[a]

assignment	λ_{max}	$\|D\| - \|E\|$	$\|D\| + \|E\|$	$\|D\|$	$\|E\|$	τ_x	τ_y	τ_z
BChl *g*[b]		470−490	930−960	700−725	230−235	0.37	0.29	1.2
BChl *g*[c]		480	925	703	223			
^{3}P	794	473	982	727.5	254.5	0.35	0.27	1.15
antenna	798−814	455−445	906−883	680−663	227−220	0.2	0.2	2.2−1.5
	814	466−476	925−935	690−705	230			1.2[d]
	800[e]	450	935	693	243			1.55

[a] The estimated error for all decay times is ±0.05 ms. λ_{max} (in nanometers) is the Q_Y-maximum in the $T - S$ spectrum obtained at the corresponding $|D| \pm |E|$ transition frequencies. The signs of D and E are chosen positive for all triplet states. [b] Dissolved in ethanol/methanol (65/35% v/v), taken from ref *38*. [c] Dissolved in toluene/pyridine (85%/15% v/v), taken from ref *38*. [d] Values obtained from the recovery curves observed at the $|D| - |E|$ transition for samples under weakly reducing conditions—dark frozen. The values of τ_x and τ_y are both 0.2−0.3 ms. [e] Tentative assigment. The value of τ_z was obtained from the recovery curves at 450 and 935 MHz for samples under weakly reducing conditions—dark frozen.

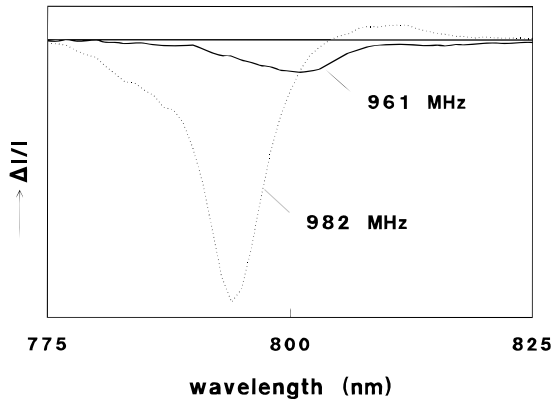

FIGURE 4: Microwave-induced $T - S$ spectrum recorded at 961 MHz (solid line) and 982 MHz (dotted line) for samples frozen during illumination under strongly reducing conditions.

than flash spectroscopy if several triplets with similar lifetimes are present.

The negative absorbance difference signals in Figure 3 at 794 nm with a shoulder at ~785 nm, and at 573 nm are attributed to the Q_Y and Q_X absorption of P, respectively. The negative signal at 725−730 nm represents a Q_Y vibronic transition, similar to that present in the absorption and $T - S$ spectra of BChl *g* (*9*, *38*, *39*).

All three spectra of Figure 3 show two positive peaks around 670 nm, superimposed on a broad positive signal between 600 and 700 nm. Because only the primary acceptor A_0, a 8^1−OH Chl *a* molecule (*12*), absorbs at this wavelength, we interpret the signal as the composite of a band shift of the Q_Y absorption of A_0 caused by a change in interaction with P upon triplet formation and a broad triplet−triplet absorption. Thus, the presence of the 670 signal corroborates our assignment of the 473, 509, and 982 MHz zf transitions to ^{3}P.

In some spectra of Figure 1, signals at ~490 and ~960 MHz, close to the signals at 509 and 982 MHz, respectively, are observed. The signals at 490/509 and 960/982 MHz are all negative, and their amplitudes vary strongly with the redox condition, indicating that the signals at 490 and 960 MHz are also associated with ^{3}P. The third zf transition at the difference frequency of 470 MHz overlaps with the 473 MHz transition and is not resolved. While the $T - S$ spectra recorded at 490 MHz (not shown) and 960 MHz (Figure 4) show the bleaching at ~800 nm expected for ^{3}P, they do not show the positive signal at 805−815 nm present in the $T - S$ spectra recorded at 509 and 982 MHz. Probably, the $T - S$ spectra recorded at 490/960 MHz and at 509/982 MHz reflect two types of RCs with a somewhat different environment or configuration of P. Such heterogeneity is also found for isolated RCs and chromatophores of purple bacteria (*40*−*42*).

The $T - S$ spectra recorded at the zf-frequencies 509 and 982 MHz assigned to ^{3}P show a positive signal between 805 and 815 nm, which we ascribe to a band shift of chromophores that are close to P. In the $T - S$ spectrum recorded at 473 MHz, the third zf-frequency of ^{3}P, the positive signal at 805−815 nm is not observed, due to the contribution of a negative signal at 814 nm, which is caused by overlap of the 473 MHz transition with the $|D| - |E|$ transition of antenna chromophores absorbing at 814 nm (see below).

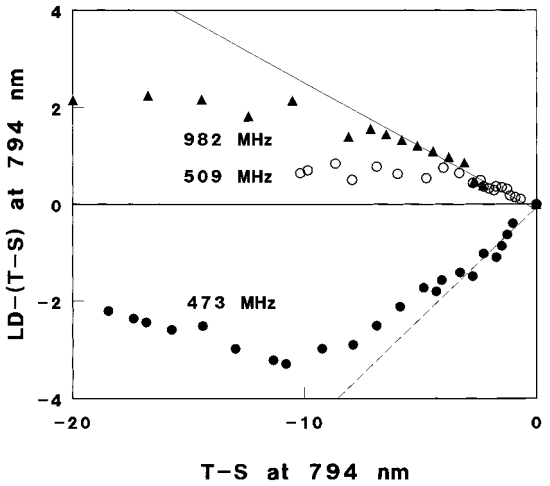

FIGURE 5: LD($T - S$) signal amplitude plotted against the $T - S$ signal amplitude recorded at 794 nm and 473 MHz (dots), 509 MHz (open circles) and 982 MHz (triangles). Extrapolation to zero-microwave power yields for the ratio of the LD($T - S$) to the $T - S$ signal values of 0.45 ± 0.05 (473 MHz) and −0.28 ± 0.05 (509 and 982 MHz), given by the slope of the straight dashed line and solid line, respectively.

Assignment of the Zero-Field Transitions of ^{3}P. We assign the resonance at 473 MHz to the $|D| - |E|$ transition, and that at 509 MHz to the $2|E|$ transition. That is, we choose the *z*-sublevel to be lowest in energy (*D* positive) and to have the longest decay time (Table 1), as usual for planar π-electron systems. To test this assumption, linear-dichroic (LD) ADMR experiments were performed, from which the orientation of the optical transition moment with respect to the triplet axes can be determined. With LD-ADMR, the $T - S$ signal parallel and perpendicular to the direction of the microwave magnetic field is measured, the difference being defined as the LD($T - S$) signal (*35*). At low microwave powers when the $T - S$ and the LD($T - S$) signals are linearly dependent, the angle α between the optical transition moment and the triplet *i*-axis is given by the relation (*43*, *44*):

$$R_i = \frac{\Delta A_{\parallel} - \Delta A_{\perp}}{\Delta A_{\parallel} + \Delta A_{\perp}} = \frac{\mathrm{LD}(T-S)}{T-S} = \frac{(3\cos^2\alpha_i - 1)}{(3 + \cos^2\alpha_i)}, \quad i = x, y, z \quad (1)$$

For the angle between the Q_Y transition moment of P (794 nm) and the 473, 509, and 982 MHz microwave transition moments, we obtained *R* values corresponding to 0−20°, 70−90°, and 70−90°, respectively (Figure 5 and Table 2).

Accepting that the Q_Y transition moment is oriented in the plane of the BChl macrocycle, the LD-ADMR results agree with the assignment of the 509 MHz resonance to the $2|E|$ transition, which is polarized along the triplet *z*-axis, taken perpendicular to the macrocycle plane for planar aromatic systems. Note that, irrespective of the geometry of P (a dimer, for instance) and of a possible exciton contribution to the Q_Y transition, the triplet *z*-axis of ^{3}P can never be oriented parallel to Q_Y of P when in monomeric BChl *g* the triplet *z*-axis is perpendicular to Q_Y.

Antenna Triplets Formed by Intersystem Crossing. Upon detection at 814 nm, the intensities of the 466−476 and 920−935 MHz zf transitions in Figure 1 were independent of the redox state of the secondary acceptors. The $T - S$ spectra

Table 2: Orientation (α) of the Q_Y-Transition Moments of the Primary Donor and the Antenna of *H. chlorum* with Respect to Their Triplet Axes, Determined at the Frequencies ν (in megahertz) Indicated

	λ_{det} (nm)	$\lvert\alpha_x\rvert$ (deg)	$\nu_{\lvert D\rvert+\lvert E\rvert}$ (MHz)	$\lvert\alpha_y\rvert$ (deg)	$\nu_{\lvert D\rvert-\lvert E\rvert}$ (MHz)	$\lvert\alpha_z\rvert$ (deg)	$\nu_{2\lvert E\rvert}$ (MHz)
P	794	70−90	982	0−20	473	70−90	509
antenna	800−808	58−65	895−906	24−37	450		
antenna	814	55−70	935	25−40	476		

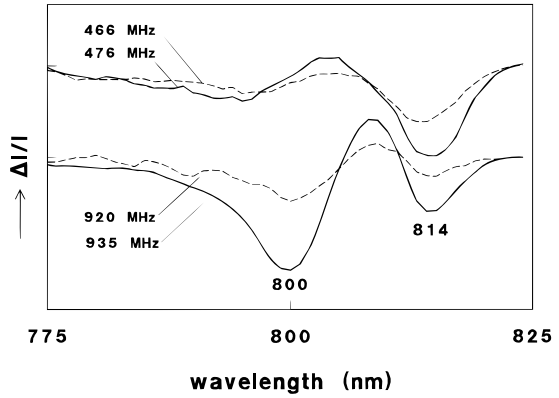

FIGURE 6: $T - S$ spectra recorded at 466 and 476 MHz and at 920 and 935 MHz for samples frozen in the dark under weakly reducing conditions.

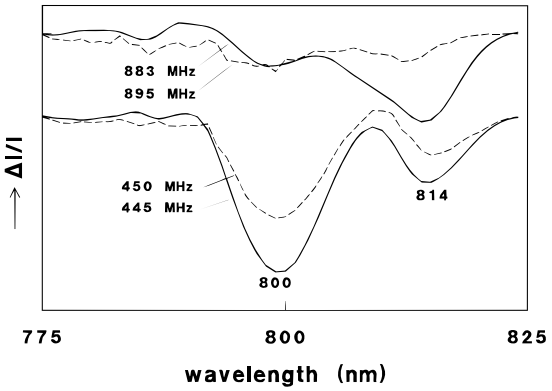

FIGURE 7: $T - S$ spectra recorded at 445 and 450 MHz and 895 and 883 MHz for samples under weakly reducing conditions and frozen in the dark.

taken at 476 and 935 MHz for weakly reducing conditions show negative signals at 795−805 and 814 nm (Figure 6). A negative signal in a $T - S$ spectrum can be due to bleaching of a chromophore band because of triplet formation, or it can be part of a band shift of a certain chromophore arising from a change in interaction between this chromophore and an adjacent chromophore. We ascribe the negative signal at 814 nm to the bleaching upon triplet formation by intersystem crossing of antenna chromphores absorbing at 814 nm, which are only weakly coupled to P. The negative signal at ~795−800 nm and the positive signal at 804−807 nm in the $T - S$ spectra of Figure 6 have the signature of a band shift of an antenna component absorbing at 795−800 nm, which interacts with the 814 nm pigment. An alternative interpretation, that the 814 nm signal is part of a band shift with the triplet located on a chromophore absorbing at 800 nm, does not fit well the $T - S$ spectra recorded at 466 and 476 MHz (Figure 6).

The response curves at 476 and 935 MHz both contain a slow component (Table 1), which we ascribe to the decay of the common triplet *z*-sublevel. Apparently, the 476 and 935 MHz bands constitute the $|D| - |E|$ and $|D| + |E|$ transition of the triplet located on the 814 nm pigments, respectively. The corresponding $2|E|$ transition at 459 MHz appears to be hidden under the signal at 466−476 MHz.

Triplet States with Zero-Field Transitions at 450 and 906 MHz. Like the intensities of the zf transitions of ^{3}P, the zf transitions at ~450 and ~906 MHz strongly depend on the redox condition (Figure 1). The relative change in intensity recorded at 800 nm shows a behavior similar to that of the zf transitions of ^{3}P recorded at 794 nm when comparing the (four) different sample conditions, as discussed below.

(a) Weakly Reducing Conditions. The $T - S$ spectra of samples frozen in the dark under weakly reducing conditions, in the absence of dithionite, are shown in Figure 7. For samples frozen in the dark in the presence of dithionite, the $T - S$ spectra were identical (not shown). The $T - S$ spectrum recorded at the $|D| - |E|$ transition at 450 MHz shows two negative signals, at 800 and 814 nm. At the $|D| + |E|$ transition, the relative amplitude of these signals depends on the microwave frequency selected. At 883 MHz, the intensity at 814 nm is relatively stronger, whereas at higher frequencies, the 800 nm component is dominant, being maximal at 906 MHz. In other words, the $|D| + |E|$ transition in the ADMR spectrum is better resolved than the $|D| - |E|$ transition (see also Figure 1 for detection wavelengths between 800 and 814 nm). The $2|E|$ transition, expected to be observable at the same frequency as the $|D| - |E|$ transition (as $|D| \approx 3|E|$), contributes little or not to the ADMR spectrum of Figure 1, because the decay times τ_x and τ_x are almost equal and much smaller than τ_z (Table 1).

From the maxima in the $T - S$ spectra, we conclude that the zf transitions discussed above arise from triplets located on the BChl *g* chromophores absorbing at 800 nm, with $|D| - |E|$ at ~450 MHz and $|D| + |E|$ at 906 MHz, and to triplet states located on the chromophores absorbing at 814 nm with zf transitions at ~445 MHz ($|D| - |E|$) and 883 MHz ($|D| + |E|$).

(b) Strongly Reducing Conditions. The $T - S$ spectrum recorded at 455 MHz (Figure 8) for samples prepared under strongly reducing conditions shows a negative signal in the Q_Y region between 798 and 808 nm, with a maximum around 800 nm. In the Q_X region, a negative signal is observed between 570 and 590 nm, which is broader and much weaker than the Q_Y band in the $T - S$ spectrum of P at 573 nm. No Q_Y signal of the primary acceptor A_0 is observed around 670 nm. Therefore, we attribute the zf frequencies around 450 MHz and between 883−906 MHz to triplet states of antenna BChl *g*.

In Figure 9, the $T - S$ spectra in the Q_Y region, recorded at the $|D| - |E|$ and the $|D| + |E|$ transitions, are shown in more detail, measured for samples under strongly reducing conditions. The wavelength of maximum absorbance difference signal depends appreciably on the microwave frequency selected. Thus, both the zf transitions and the

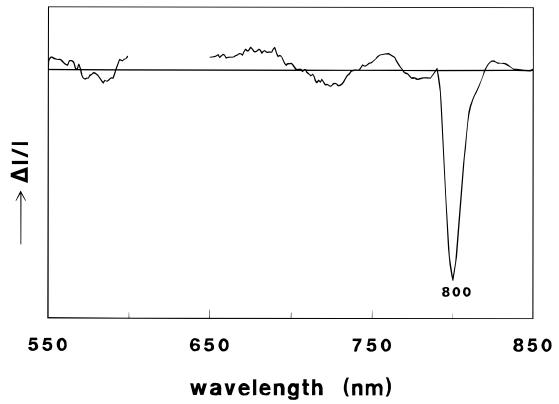

FIGURE 8: $T - S$ spectrum recorded at 455 MHz for samples frozen under illumination under strongly reducing conditions.

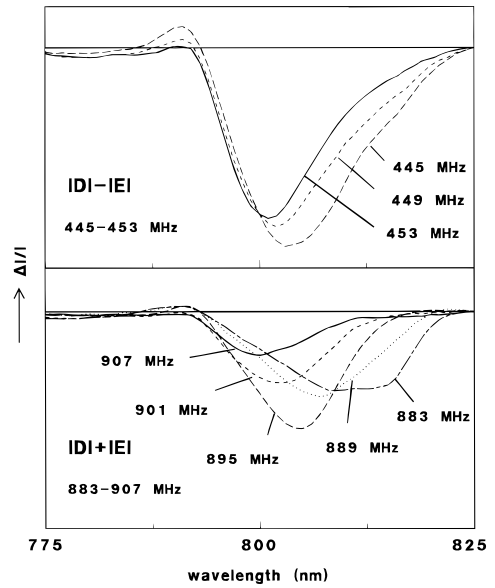

FIGURE 9: $T - S$ spectra recorded at 445−453 (top) and 883−906 MHz (bottom) for samples frozen under illumination under strongly reducing conditions.

optical Q_Y and Q_X signals reflect a relatively large heterogeneity. In contrast to the two well-resolved bands at 800 and 814 nm in the spectra recorded at 445−450 MHz for weakly reducing conditions (Figure 7), for the samples under strongly reducing conditions, Figure 9 shows single, broad absorption bands. This apparent decrease in resolution is caused by the strong increase of the 800 nm band for strongly reducing conditions, while the band at 814 nm is redox insensitive. The increase in the signal when the same sample is frozen under illumination depends on the detection wavelength. The increase is largest for pigments absorbing at short wavelengths (798−802 nm), with a $|D| + |E|$ transition at 906 MHz, and is then similar to the increase found for the concentration of ^{3}P.

With LD-ADMR spectroscopy, we found for the 800 nm component R values of 0.32 ± 0.07 and -0.10 ± 0.05 at 450 and 906 MHz, respectively (data not shown), yielding the orientation of the Q_Y transition moment of the 800 nm antenna chromophores with respect to their triplet axes, listed in Table 2. A similar orientation was obtained for the 814 nm antenna pigments (Table 2).

Decrease of Triplet Concentration by Illumination at 1.2 K. A remarkable result is that the triplet concentration for the chromophores absorbing around 800 nm (with zf transitions at 450 and 906 MHz) is sensitive to illumination at 1.2 K. After illumination for 0.5−1 h, the intensities of the zf transitions at 450 and 906 MHz decrease to 50−60% of their original value and remain constant afterward. This is depicted in Figure 10 for the $|D| - |E|$ region. In contrast, the intensities of the zf transitions of ^{3}P at 473 and 509 MHz (Figure 10) and 982 MHz (not shown) and of the zf transitions of the triplet of the 814 nm antenna at 466−476 and 925−935 MHz remain constant. The effect of prolonged illumination at 1.2 K on the triplet concentration of the 800 nm (450 and 900 MHz) antenna is reversible when the samples were warmed to above liquid nitrogen temperature (about 90−100 K) and subsequently refrozen in the dark, and can therefore not be attributed to (photo)damage of (antenna) BChl *g*. Because the initial intensities of the triplet signals were restored, this experiment indicates that warming to 90−100 K and subsequent cooling to 1.2 K, keeps the initially reduced secondary acceptors in the reduced state. The effect was stronger for the short-wavelength components (probed at 798 nm) of the 800 nm band than for its longer-wavelength components (probed at 808 nm). For weakly reducing conditions (dark-frozen), the decrease of signal intensity after prolonged illumination was also observed, but only for the 800 nm component in the spectra recorded at 450 and 906 MHz (Figure 7). A similar effect has been observed at 800 nm by Nitschke et al. (*21*) using nanosecond laser flashes, continuous illumination at low temperature (10 K), and weakly reduced samples. From EPR data on the reduced iron−sulfur centers, Nitschke et al. (*21*) attributed the effect to the generation of a stable (up to 100 K) ion pair involving P and a terminal acceptor (an iron sulfur center). We believe that our results originate from the formation of a similar ion pair, however, not involving one of the secondary acceptors (see Discussion). We emphasize that neither for ^{3}P nor for the triplet state of the 814 nm absorbing antenna did we observe any light-induced decrease of the concentration (see above).

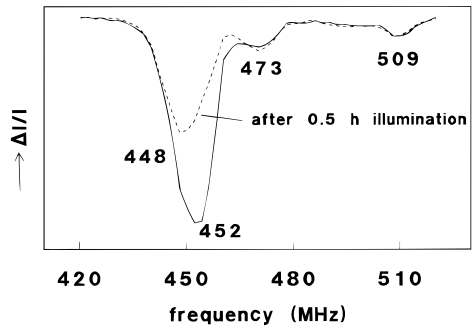

FIGURE 10: Change in transmittance at 800 nm as a function of the microwave frequency at the start of illumination (solid line) at 1.2 K and after 30 min of illumination (dashed line) for samples frozen under illumination under strongly reducing conditions.

DISCUSSION

The Triplet State of BChl g in H. chlorum. We first note that the values of $|D|$ and $|E|$ for the triplet state of BChl *g* in organic solvents and for the triplet states in membranes of *H. chlorum* are very close (Table 1). The similarities of ^{3}BChl *g* in organic solvents and ^{3}P in membranes of *H. chlorum*, as regards the sublevel decay rates and $|D|$ values,

make it plausible that the triplet state of P is localized on a single BChl *g* molecule.[2] The higher $|E|$ value of ^{3}P as compared to that of ^{3}BChl *g* in organic solvents may be attributed to a difference in coordination of the central magnesium atom. An indication for this is the position of the Q_X absorption band of BChl *g* in ethanol/methanol at 595 nm and in toluene/pyridine at 605 nm (*38*), which differs considerably from that in the $T - S$ spectrum due to ^{3}P formation (573 nm). In ethanol at low temperature and in strongly coordinating pyridine, (B)Chls are mainly biligated, which is reflected by a Q_X absorption centered at relatively long wavelengths and by a relatively low $|E|$ value (*45*, *46*). Thus, the BChls of P are probably monoligated.

Contrary to the present findings, on the basis of EPR data, Nitschke et al. (*21*) ascribed the triplet with $|D|$ value of 727.5 MHz to the antenna absorbing at 814 nm and the triplet having $|D| = 678$ MHz to the RC. From our results in zero-magnetic field, it is clear that the interpretation of the 9 GHz EPR data is complicated by the fact that $|D|$ equals about $3|E|$ for all triplets in *H. chlorum* and that the signals of the various triplet states overlap in the EPR spectra. However, the results of Nitschke et al. (*21*) and our results agree with respect to the influence of the sample conditions on the concentration of the triplet state with a $|D|$ value of 663−680 MHz.

For BChl *g* in organic solvents as well as in *H. chlorum*, we find a relatively high value of $|E|$, quite unlike the values of $|E|$ of other (B)Chls (*47*). This high value may be caused by the presence of a vinyl group at position 3 on ring I, which is not found in BChl *a* and BChl *b*. A notable feature is the high intensity of the $2|E|$ transition for ^{3}P compared to ^{3}BChl *g* and ^{3}BChl *a*,*b* in organic solvents, whose $2|E|$ transitions are not observable by ADMR (*38*). The relatively high intensity of the $2|E|$ transition of ^{3}P may be caused by a difference in sublevel populating probabilities for ^{3}P and monomeric ^{3}BChl *g* in organic solvents. This is not unlikely, as the triplet state of P is formed via radical recombination, whereas the triplet state of BChl in vitro is formed via intersystem crossing with different sublevel selection rules. The remarkably large intensity of the $2|E|$ transition observed for ^{3}P of *H. chlorum*, however, stands in contrast to the very weak $2|E|$ intensity of ^{3}P in other RCs. Possibly, the high value of $2|E|$, which is larger than the value of $|D| - |E|$ ($|D| < 3|E|$), and the relatively strong intensity of the $2|E|$ transition have related causes.

The LD-ADMR results for P and the antenna chromophores listed in Table 2 confirm that the bands between 400 and 500 MHz of the triplet states of the antenna pigments mainly represent $|D| - |E|$ transitions. The significantly different orientation of the Q_Y transition moments of P and of the antenna with respect to their triplet axes may be attributed to environmental effects. A change in orientation of the transition moments of Chl *a* with respect to its in-plane triplet axes has been observed for different organic solvents (*38*). Likewise, we attribute the differences between the triplet-sublevel decay rates and zfs parameters of ^{3}P and the antenna triplet states to different environments of the triplet-carrying molecules.

[2] The *D*-value of a planar, strictly parallel dimer is also identical to that of the constituting monomers.

The $T - S$ Spectrum Associated with ^3P. In the ^{3}P-associated $T - S$ spectra of Figure 3, we may ascribe the 785 nm shoulder and the weak positive band around 765 nm to band shifts of BChl *g* chromophores that are located close to P. In the P^+X^--PX spectrum of *H. chlorum* (X represents a secondary acceptor), a band shift at ∼780 nm is attributed to an electrochromic shift of an absorption band of a BChl *g* pigment that is close to the primay donor (*17*, *28*).

The broad positive signal between 600 and 650 nm is similar to that found for BChl *g* in organic solution (*38*), and we attribute it similarly to triplet−triplet absorption. We ascribe the small positive band at the long-wavelength side of the Q_Y signal of P (805−815 nm), found when recording the $T - S$ spectra at 509 and 982 MHz, to a band shift of (antenna) BChl *g* chromophores that are closely connected with P, because it depends similarly on the redox conditions as all other signals in the ^{3}P-associated $T - S$ spectrum. Note that this positive signal is not observed when recording the $T - S$ spectrum at 473 MHz because of overlap with a zf transition of the 814 nm antenna (see Results). Similarly, the positive contribution at 790−792 nm in the $T - S$ spectra of Figure 9, which is most pronounced when the maximum bleaching peaks around 802−806 nm and is only present under strongly reducing conditions (light-frozen), may reflect an interaction between the antenna absorbing at 798−808 nm and P (see also below). When the ^{3}P-associated $T - S$ spectrum is recorded at 960 MHz (Figure 4) instead of 982 MHz, no band shift is observed at 805−815 nm. Apparently, in RCs with zf transitions at 960 MHz, the interactions between P and neighboring chromophores are smaller than for RCs having zf transitions at 982 MHz.

Around 670 nm, two bands are observed in Figure 3, which we interpret to represent a red-shift to 670 nm and a blue-shift to 662 nm, due to the presence of two 8^1−OH Chl *a* molecules serving as the primary acceptors and showing a maximum bleaching at 666 nm in the $P^+A_0^-$-PA_0 spectrum (*15*, *17*). Accepting a localized triplet state of P (see above), the homodimeric symmetry is broken when P is excited to the triplet state. Because the two acceptor chlorophylls must have a different distance to each of the dimer-halves of P, their interaction with ^{3}P and the corresponding band shift are expected to differ also. Note that, because of the (presumed) strict C_2 symmetry of P and its environment, ^{3}P must be localized on each dimer-half in equal proportion so that the band shifts of the two A_0 molecules will have equal intensity. We note that the signal between 660 and 675 nm is very similar to that observed in the $T - S$ spectrum of P_{700} of plant photosystem I (*31*).

Antenna Absorbing at 814 nm. The maximum of the Q_Y transition (at 814 nm) in the $T - S$ spectra recorded at 466−676 and 925−935 MHz (Figure 6) is at the same wavelength as found with pump−probe measurements on a picosecond time scale (*15*, *48*). The relatively small width of the 814 nm band compared to that found for the total 808 nm band in steady-state absorption indicates that the 814 nm component is composed of BChl molecules with a distribution of partly overlapping Q_Y maxima that is much narrower than that of the 808 nm BChls. Because the triplet yield of the 814 nm antenna is independent of the redox conditions under which the sample is prepared, we conclude that they are not connected with the primary donor. Possibly, they represent

a fraction of the antenna with a relatively long fluorescence lifetime (*49*). The picture which emerges is that a fraction of the antenna BChls transfer their excitations to the 814 nm antenna pigments, which subsequently decay by fluorescence or by intersystem crossing to their triplet state, but which do not transfer their excitation to the primary donor at cryogenic temperatures.

The Influence of the Redox Condition on the Triplet Concentration. The increase of the population of ^{3}P with the concentration of reduced secondary acceptors can be ascribed to the expected increase of the triplet yield due to inhibition of secondary electron transport, and the stimulation of recombination of $P^+A_0^-$ to ^{3}P. The concentration of ^{3}P and of the triplet states with zero-field transitions at ∼450 and 906 MHz are influenced in a comparable way by the reduction state of the secondary acceptors. This observation can be explained by assuming that the latter signals arise from antenna chromophores absorbing around 800 nm that are closely connected to P. Closing P for antenna excitations by ^{3}P formation enhances their lifetime, and thus the probability of triplet formation on the 800 nm antenna. The influence of the redox state on the antenna triplet concentration is largest for the antenna absorbing at 798−802 nm and gradually diminishes for the antenna absorbing at longer wavelength. This is not surprising since the antenna pigments absorbing around 800 nm should be more efficient in energy transfer to the RC than those absorbing at longer wavelength. This heterogeneity in energy-transfer properties and the heterogeneity observed in the $T - S$ spectra (Figure 9) and zf transitions (Figure 1) probably correspond to the heterogeneity that causes the range of fluorescence lifetimes (25−900 ps) associated with different wavelengths of fluorescence (*49*).

Light-Induced Stable Charge Separation at 1.2 K. The decrease of the intensity of the zf transitions recorded in the 800 nm region during prolonged illumination at 1.2 K most likely can be attributed to an effect of stable charge separation involving P and an acceptor (see Results) on the triplet concentration of the 800 nm antenna. Stable charge separation will progressively increase the P^+ concentration and consequently will indirectly decrease the triplet concentration of the antenna via quenching of the antenna singlet excitations by P^+ (*50*). The precursor state of the stable charge separation does not quench antenna excitations (the initial yield of antenna triplets is high), so it cannot contain P^+, PA_0 or PA_0A_1. It also cannot form or contain ^{3}P as the ^{3}P yield is not affected by prolonged illumination at 1.2 K. It is therefore unlikely that the stable ion pair contains one of the reduced secondary acceptors of the normal acceptor chain. We propose that the precursor state is composed of $PA_0^-A_1^-$... Illumination will bring about an equilibrium between the excited states of P and the antenna chromophores, with high probability of forming antenna triplet states (not ^{3}P because of the predominance of antenna pigments over P). With low yield, the stable ion pair P^+Q^- is formed, with Q a low quantum yield acceptor aside of the normal electron transport chain. A candidate for Q is the menaquinone that can be reduced by photoaccumulation (*19, 20*) but does not appear to function in the normal acceptor chain (*26*) (see, however, ref *51*). The ion pair quenches antenna excitations, thus gradually reducing the concentration of antenna triplets. Note that the yield of ^{3}P, formed in RCs in the state $PA_0\ A_1^-$, is not affected, because here the lifetime of the excited state of P is much shorter than when A_0 is also reduced, so that the probability of creating the ion pair P^+Q^- is greatly diminished in this fraction of the RCs.

CONCLUSIONS

With ADMR in zero magnetic field, we have characterized the triplet states in *H. chlorum* residing on the antenna chromophores and on the primary donor. From a comparison of the $T - S$ spectra obtained at the various observed ADMR frequencies, the zfs-parameters of ^{3}P could be unequivocally determined, being 727.5 MHz (0.0243 cm^{-1}) and 254.5 MHz (0.0085 cm^{-1}) for $|D|$ and $|E|$, respectively. The low value of $|E|$ suggests that the BChls of P are monoligated. The ^{3}P-associated $T - S$ spectra and the zf transitions show relatively narrow line widths. A fraction of the primary donor, present to a minor extent, has slightly different zfs-parameters and optical properties. From the $T - S$ spectra, we conclude that this minor fraction has a different interaction with nearby (antenna) chromophores than the majority of P.

Several triplet states of the antenna have been observed, which are located on BChl *g* molecules absorbing at longer wavelength than the primary donor. This finding agrees with earlier observations that the excitation energy transfer from the antenna to the RC is not 100% efficient under the conditions used (*4, 52, 53*). The range of zfs-parameters and Q_Y maxima of the antenna indicate that in membranes of *H. chlorum* the antenna are heterogeneous. This heterogeneity was also observed in the efficiency of energy transfer to the RC. The zfs-parameters of all triplet states are similar to those found for monomeric BChl *g* in organic solvents, from which we conclude that the triplet states are localized on single BChl *g* chromophores. The differences in zfs-parameters, decay rates, and the orientation of the triplet axes with respect to the Q_Y transition moments are ascribed to variation in the environment of the triplet-carrying molecules.

Under strongly reducing conditions, we have observed an increase of the concentration of part of the antenna triplets, from which we conclude that part of the RCs is closed under these redox conditions. Prolonged illumination at 1.2 K caused a decrease of the aforementioned enhanced antenna triplets. We ascribe this effect to the creation of a stable ion pair in the RC, involving P^+ and a reduced, low-quantum yield acceptor on a side path, possibly a menaquinone.

The striking similarities between the spectral properties of ^{3}P of *H. chlorum* and $^3P_{700}$ of photosystem I of plants and between the triplet-induced absorbance changes in the spectral region of the Q_Y band of the primary acceptor of the two photosystems strongly support the notion that membrane fragments of the Heliobacteriacea are a useful model system for the more complicated RC of photosystem I, with a cofactor architecture that is very close to that of the latter RC.

ACKNOWLEDGMENT

We thank Stephan Otte for providing the low-temperature absorption and fluorescence data. Rob Louwe is acknowl-

edged for useful discussion. We thank Profs. J. Amesz and J.H. van der Waals for their interest and helpful suggestions.

REFERENCES

1. Brockmann, H., and Lipinski, A. (1983) *Arch. Microbiol. 136*, 17−19.
2. Madigan, M. T. (1995) in *Anoxygenic Photosynthetic Bacteria* (Blankenship, R. E., and Madigan, M. T., Eds.) pp 17−30, Kluwer Academic Publishers, Dordrecht.
3. Gest, H., and Favinger, J. L. (1983) *Arch. Microbiol. 136*, 11−16.
4. Amesz, J. (1995) in *Anoxygenic Photosynthetic Bacteria* (Blankenship, R. E., and Madigan, M. T., Eds.) pp 687−697, Kluwer Academic Publishers, Dordrecht.
5. Woese, C. R., Debrunner-Vosbrink, B. A., Oyaizu, M., Stackebrandt, E., and Ludwig, W. (1985) *Science 229*, 762−765.
6. Trost, J. T., and Blankenship, R. E. (1986) *Biochemistry 28*, 9898−9904.
7. van de Meent, E.-J., Kleinherenbrink, F. A. M., and Amesz, J. (1990) *Biochim. Biophys. Acta 1015*, 223−230.
8. Liebl, U., Rutherford, A. W., and Nitschke, W. (1990) *FEBS Lett. 261*, 427−430.
9. Kobayashi, M., van de Meent, E.-J., Erkelens, C., Amesz, J., Ikegami, I., and Watanabe, T. (1991) *Biochim. Biophys. Acta 1057*, 89−96.
10. Kobayashi, M., Wanatabe, T., Ikegami, I., van de Meent, E. J., and Amesz, J. (1991) *FEBS Lett. 284*, 129−131.
11. Takaichi, S., Inoue, K., Akaike, M., Kobayashi, M., Oh-oka, H., and Madigan, M. (1997) *Arch. Microbiol. 168*, 277−281.
12. van de Meent, E.-J., Kobayashi, M., Erkelens, C., van Veelen, P. A., Amesz, J., and Watanabe, T. (1991) *Biochim. Biophys. Acta 1058*, 356−362.
13. van de Meent, E.-J., Kobayashi, M., Erkelens, C., van Veelen, P. A., Otte, S. C. M., Inoue, K., Wanatabe, T., and Amesz, J., (1992) *Biochim. Biophys. Acta 1102*, 371−378.
14. Nuijs, A. M., van Dorssen, R. J., Duysens, L. N. M., and Amesz, J. (1985) *Proc. Natl. Acad. Sci. U.S.A.* 82, 6865−6868.
15. van Kan, P. J. M., Aartsma, T. J., and Amesz, J. (1989) *Photosynth. Res. 22*, 61−68.
16. Lin, S., Chiou, H.-C., Kleinherenbrink, F. A. M., and Blankenship, R. E. (1994) *Biophys. J. 66*, 437−445.
17. Kleinherenbrink, F. A. M., Aartsma, T. J., and Amesz, J. (1991) *Biochim. Biophys. Acta 1057*, 346−352.
18. Prince, R. C., Gest, H., and Blankenship, R. E. (1985) *Biochim. Biophys. Acta 810*, 377−384.
19. Brok, M., Vasmel, H., Horikx, J. T. G., and Hoff, A. J. (1986) *FEBS Lett. 194*, 322−326.
20. Smit, H. W. J., Amesz, J., and van der Hoeven, M. F. R. (1987) *Biochim. Biophys. Acta 893*, 232−240.
21. Nitschke, W., Sétif, P., Liebl, U., Feiler, U., and Rutherford, A. W. (1990) *Biochemistry 29*, 11079−11088.
22. Fischer, M. R. (1990) *Biochim. Biophys. Acta 1015*, 471−481.
23. Trost, J. T., Brune, D. C., and Blankenship, R. E. (1992) *Photosynth. Res. 32*, 11−22.
24. Kleinherenbrink, F. A. M., Chiou, H.-C., LoBrutto, R., and Blankenship, R. E. (1994) *Photosynth. Res. 41*, 115−123.
25. Hiraishi, A. (1989) *Arch. Microbiol. 151*, 378−379.
26. Kleinherenbrink, F. A. M., Ikegami, I., Hiraishi, A., Otte, S. C. M., and Amesz, J. (1993) *Biochim. Biophys. Acta 1142*, 69−73.
27. van Dorssen, R. J., Vasmel, H., and Amesz, J. (1985) *Biochim. Biophys. Acta 809*, 199−203.
28. Smit, H. W. J., van Dorssen, R. J., and Amesz, J. (1989) *Biochim. Biophys. Acta 973*, 212−219.
29. Kleinherenbrink, F. A. M., Deinum, G., Otte, S. C. M., Hoff, A. J., and Amesz, J. (1992) *Biochim. Biophys. Acta 1099*, 175−181.
30. Hoff, A. J. (1996) in *Biophysical Techniques in Photosynthesis* (Amesz, J., and Hoff, A. J., Eds.) pp 277−298, Kluwer Academic Publishers, Dordrecht.
31. Vrieze, J., Gast, P., and Hoff, A. J. (1996) *J. Phys. Chem. 100*, 9960−9967.
32. Hoff, A. J. (1990) in *Physical Methods in Plant Sciences, Vol. II, Modern Methods of Plant Analysis* (Linskins, H. F., and Jackson, J. F., Eds.) p 23, Springer-Verlag, Berlin.
33. Hoff, A. J. (1993) in *Metallobiochemistry Part D, Methods in Enzymology, Vol. 227* (Riordan, J. F., and Vallee, B. L., Eds.) p 290, Academic Press, San Diego.
34. den Blanken, H. J., and Hoff, A. J. (1982) *Biochim. Biophys. Acta 681*, 365−374.
35. den Blanken, H. J., Meiburg, R. F., and Hoff, A. J. (1984) *Chem. Phys. Lett. 105*, 336−342.
36. van der Vos, R., Carbonera, D., and Hoff, A. J. (1991) *Appl. Magn. Res. 2*, 179−202.
37. Otte, S. C. M., van der Heiden, J. C., Pfenning, N., and Amesz, J. (1991) *Photosynth. Res. 28*, 77−87.
38. Vrieze, J., and Hoff, A. J. (1995) *Chem. Phys. Lett. 237*, 493−501.
39. Vrieze, J., van de Meent, E.-J., and Hoff, A. J. (1992) in *The Photosynthetic Bacterial Reaction Center. Structure and Dynamics* (Breton, J., and Verméglio, A., Eds.) pp 67−77, Plenum Press, New York.
40. den Blanken, H. J., and Hoff, A. J. (1983) *Chem. Phys. Lett. 98*, 255−262.
41. Owen, G. M., Jones, M. R., and Hoff, A. J. (1997) *J. Phys. Chem. 101*, 7197.
42. Gast, P., Lous, E. J., and Hoff, A. J. (1995) *Chem. Phys. 194*, 387.
43. Meiburg, R. F. (1985), Ph.D. Thesis, Leiden University, The Netherlands.
44. Verméglio, A., Breton, J., Paillotin, G., and Cogdell, R. (1978) *Biochim. Biophys. Acta 501*, 514−530.
45. Angerhofer, A., von Schütz, J. U., and Wolf, H. C. (1988) *Chem. Phys. Lett. 151*, 195−198.
46. Renge, I., and Avarmaa, A. (1985) *Photochem. Photobiol. 42*, 253−260.
47. den Blanken, H. J., and Hoff, A. J. (1983) *Chem. Phys. Lett. 96*, 343−347.
48. van Noort, P. I., Aartsma, T. J., and Amesz, J. (1994) *Biochim. Biophys. Acta 1184*, 21−27.
49. Kleinherenbrink, F. A. M., Cheng, P., Amesz, J., and Blankenship, R. E. (1993) *Photochem. Photobiol. 57*, 13−18.
50. Deinum, G., Kleinherenbrink, F. A. M., Aartsma, T. J., and Amesz, J. (1992) *Biochim. Biophys. Acta 1099*, 81−84.
51. Chiou, H. C., and Blankenship, R. E. (1997) *Photochem. Photobiol. 64*, 32−37.
52. Liebl, W., Lambry, J. C., Breton, J., Martin, J.-L., and Vos, M. H. (1997) *Biochemistry 36*, 5912−5920.
53. Chiou, H. C., Lin, S., and Blankenship, R. E. (1997) *J. Phys. Chem. B 101*, 4136−4141.

BI981207W